

New Integrated Cermet Powder Preparation and Consolidation Method – Ni-ZrO₂ Case

Thomaz Augusto Guisard Restivo^{1,a}, Sonia Regina Homem Mello-Castanho^{1,b}

¹Nuclear and Energetic Research Institute – IPEN - Av. Lineu Prestes 2242 – 05508000 – São Paulo – Brazil

^aguisard@dglnet.com.br, ^bsrmello@ipen.br

Keywords: cermet, sintering, kinetics, SOFC

Abstract. A new integrated method for direct preparation of cermet materials is proposed consisting of a powder processing method allied to a special sintering step. The powder is obtained by mechanical alloying route where a specific morphologic design is searched to yield thin metal plated ceramic particles. These have the proper characteristics to engage the sintering by activated surface (SAS) consolidation method. The last is triggered by partial evaporation and reactive sintering of thin metal layers, therefore exposing high active surfaces with superior sinterability. Refractory sacrifice metal components are found to play an important role. The application of the integrated method to Ni-ZrO₂ cermet with selected metal additives is investigated. Sintering temperatures can be reduced by more than 300°C for the same final density range. The resulted powders and pellets microstructures are analysed accordingly to the projected expected ones. The thermophysical and electrical properties measurements are performed for evaluate phases percolation.

Introduction

Cermet materials combine opposite properties from metals and ceramics, being the key components to drive new applications in several engineering areas. One known example is the cermets based on metallic nickel and yttria stabilized zirconia (Ni-YSZ) applied as the anode component of solid oxide fuel cells (SOFC) [1,2]. High temperature electrolysis (HTE) have been considered as a economic method for hydrogen production, since external heat sources from a nuclear reactor can be employed with advantages [3-5], where Cu-YSZ cermet cathodes can be viable [6]. The suitability of such cermets materials arises from their mixed electronic-ionic conduction paths, as well as the catalytic and biofuels reforming capability, giving rise to adopting of reusable energy cycles.

The powder preparation route employed in this work is based on mechanical alloying of the constituent powders, say, the ceramic and the metallic ones. The literature search found two groups publishing works where the MA processing is used for this purpose: the first one deals with high temperature water electrolysis cathodes of Ni(Cu)-YSZ [7-9] and the second one with SOFC Ni-YSZ anode [10]. However, the last has reported the material preparation was not successful for Ni content over 20% in volume, which does not comply with the electronic percolation requirements of the SOFC anodes. A further article investigates the preparation of the ceramic composite NiO-YSZ [11], which must be reduced under hydrogen during 4 hours to obtain the final cermet. Our previous articles have been demonstrated the MA can be successfully used to obtain porous cermets directly from metallic and ceramic starting powders at lower sintering temperatures [12,13]. Other advantages of the method are found to be the lower sintering temperature (1000-1200°C/ 1h) and the absent of pore-forming additives. Moreover, in the present case, the mechanical alloying route seeks a powder morphology where the metal and ceramics phases are intimately mixed, such as by embedding the ceramic particles under thin metallic films. This powder structure displays higher

sinterability and allow the onset of the sintering by activated surface (SAS) consolidation process, directly leading to porous cermets with good properties. The SAS process is a new concept that states the high active ceramic surfaces are exposed during the sintering heat cycle in order to trigger the densification at lower temperatures. Adherent metallic films of selected additives, microforged by MA, are effective on blocking the surface diffusion that reduces the powder activity at medium temperatures. The process is driven in such a way to fill the micro-sized and nano-sized superficial defects. During the sintering cycle, such surfaces are exposed by mechanisms like volatile oxides evaporation, limited coarsening, solving and reactive sintering, understood the mechanisms occur at some intermediate temperature at the range 600-1200°C. Once the SAS consolidation is strongly dependent on the additive type and on the particular process method, it has been referred to an integrated process, where the powder preparation, morphology, sintering conditions and densification are coupled for a specific cermet powder.

The work shows the SAS integrated process development for preparation of YSZ-based cermets with Ni and Cu, Ag, Mo and W as additives, which can find applications as SOFC anodes or HTE cathodes. The first selected additive - Cu - is expected to avoid carbon deposition [14,15] and increase the electrical conductivity. The second additive is chosen into the refractory metals group (Mo, W, Nb, Ta) and Ag accordingly to their ability on triggering the SAS process, besides low Cu alloy solubility and similar hydride formation enthalpy as Ni [16]. The approach is based on thermodynamics of immiscible systems on considering the repulsive interaction between Cu and C, as seen during the carbothermic alumina reduction into a Cu molten bath [17,18]. The consequence is Cu opposes to C deposition (coke poisoning) at the electrode surface. By the other side, Cu and Ni form easily an alloy at high temperatures, decreasing the own Ni activity and harming the C repulsion effect. Therefore, a second metallic additive is mixed in order to repulse itself the Cu atoms at a precipitated state. It must be emphasized the MA powder preparation method is ideal in order to homogenize ceramic and metallic powder with different densities and surface properties.

Experimental

The starting powders were a cubic stabilized zirconia with 8 mols% yttria (YSZ, Tosoh Co.), BET 13 m²/g, d(50)= 0,3µm and 2 types of metallic Ni: d(50)= 27µm atomized, 99,7w% pure and a high purity Ni powder (99,9w%, Aldrich) d(50)= 3µm, as well as the Cu powder, while W and Mo additives had average particle sizes of 5µm. The high energy milling (MA) was carried out at shaker mills rated at 19Hz with tool steel vials and AISI 52100 spheres φ5mm as milling media with balls to powder ratio of 10:1. The loaded vials were sealed under vacuum and submitted to the milling process during 3 to 8 h. The resulted contamination is limited to low Fe and Cr contents (0.3w%). Three kind of samples were prepared whose compositions were set to 40% metal content and 60% YSZ (volume %): 40%Ni, 28%Ni-12%Cu and 20%Ni-12%Cu-8%Me, Me being the refractory metal or Ag. The MA processing sequence employed (((YSZ+Ni)+Me)+Cu), 1 hour milling each pair, referred as Cu-Me-Ni-YSZ. An inverse sequence (Ni-Me-Cu-YSZ) was also prepared. Some samples employed starting Ni and Mo powders annealed at 750 and 1100°C, respectively, in H₂/Ar atmosphere during 1,5 hour. The powder samples were pressed uniaxially under 150 MPa load into 7 and 10mm diameter dies.

The SAS process was carried out at a tubular furnace under argon flow (150mL/min) with 2, 5 and 10 vol% water vapour by saturating the inlet flow line in a distilled water flask at a controlled temperature. The oxygen partial pressure was estimated through thermodynamic calculation related to water vapour decomposition at each sintering temperature. All the experiments were performed at a 10°C/min heating rate and 1-h isotherm at the maximum temperature. The powders and pellets were analysed at scanning and transmission electron microscopes and X-ray diffraction (Cu Kα). One important tool allowing to support the result analyses is the sintering kinetics by the stepwise isothermal dilatometry (SID) method. The experiments were done at a Setaram TMA/dilatometer

(Labsys TMA 1400°C) under small load (2g). The SID analysis is based on the quasi-isothermal dilatometry [19-27], where several 15-min isotherms are programmed at 50°C intervals during heating at 10°C/min along the length of the relevant temperature range. The equationing was shown in a previous paper [12-13,22-23], allowing determining the apparent activation energy of sintering.

The electrical and thermal conductivity were determined for some samples. The first one was measured by the 4-point probe method under an atmosphere Ar-5%H₂. The thermal conductivity was estimated by the flash method at a diffusivimeter built by the author with high power xenon flash (5000J) and MCT detector. The thermal quadrupole method [28,29] was applied to estimate the thermal diffusivity (α) from which the conductivity can be determined by Eq.1, while the heat capacity (Cp) is evaluated by thermodynamic tables [30] and density (ρ) is measured:

$$\lambda(T) = a(T).Cp(T).\rho(T) \quad (1)$$

Results and Discussion

Fig. 1 shows some aspects of the MA powders revealing the pursued pod-like morphology assumed besides some rather equiaxial features. One can see there are some particles embedded under metal layers or incrusted on them at a very texturized structure. In some cases, it is not possible to distinguish between the metallic and ceramic phases through SEM magnification. TEM images show the dispersion is however verified at the nanometric range (Fig. 2).

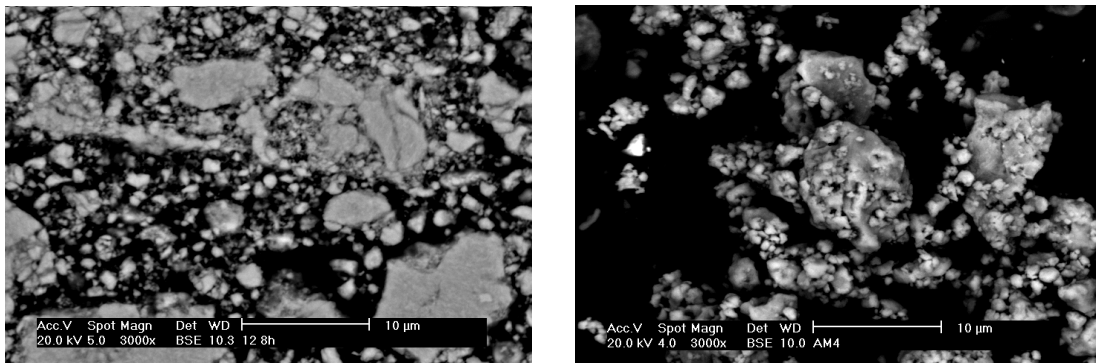


Fig. 1. MA powders morphology by SEM/BSE, compositions in vol%: right: 40Ni(28µm)-YSZ 8h MA left: 8Mo-12Cu-20Ni-YSZ 3h MA

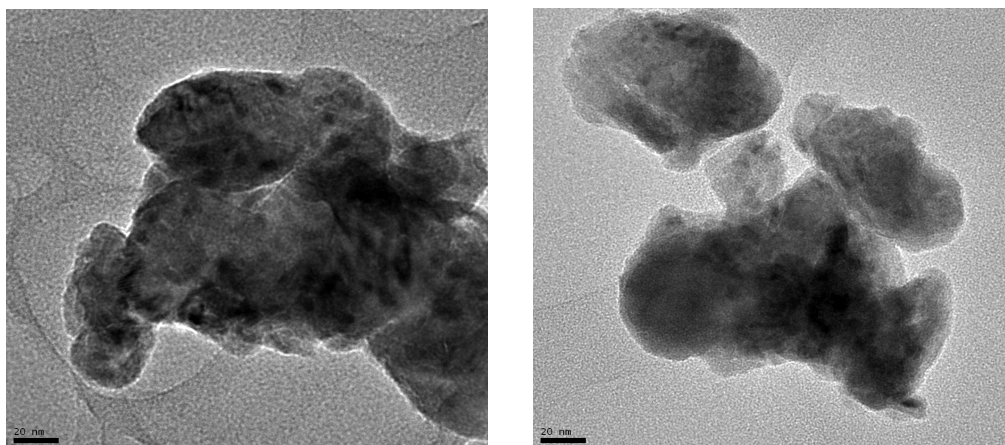


Fig. 2. Ni-YSZ powder TEM images; nanometric Ni particles appears as dark marks and lines.

The powder X-ray diffractograms in Fig. 3 compare the cermet sample with Cu and refractory metals additives. The absent of the Cu peak in Cu-Ni-YSZ sample indicates it forms an alloy with Ni. Conversely, the addition of Mo and W has preserved some precipitated Cu and its corresponding reflection. The annealing of row powders leads to less crystalline material in the forward milling sequence through the development of a defective structure. Especially the Ni peaks are attenuated which can be explained by mixing and alloying easiness of soft metal powders. The inverse milling sequence shows Ni and Mo metals more crystalline since they were milled less time. The best separation of Cu peak was found with row powders and 28 μ m Ni initial particle size.

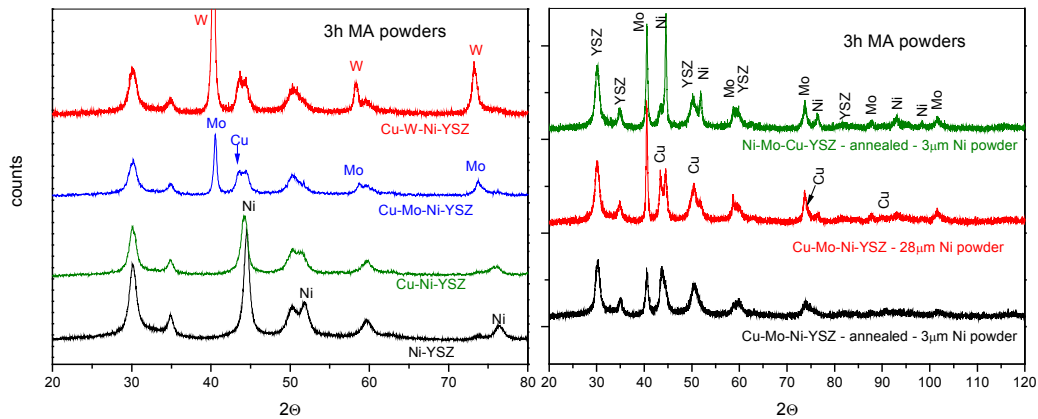


Fig. 3. Compilation of MA milled powders x-ray diffraction.

The effect of Cu and Mo additives on sintering behavior is evaluated by SID kinetic method. Fig. 4 shows the Arrhenius plots and the apparent activation energies for the sample classes. The additives are found to promote progressively the sintering process according to smaller activation energies. Cu appears to favor a low temperature sintering process, while Mo reduce the activation energy to a very low level at high temperature. Actually, Mo metal can form a volatile oxide that is expected to trigger the SAS process, in agreement to its original concept. Sintering results in tubular furnace as a function of temperature and oxygen partial pressure is shown in Fig. 5. Most samples attain suitable densities above 60%TD earlier at 1000°C/1h sintering. These results signify a sintering temperature reduction about 300°C compared to the conventional Ni-YSZ anode fabrication process. Limited PO_2 are beneficial for sintering compared to argon inert gas ($PO_2 \sim 0$) due to the mentioned SAS effect.

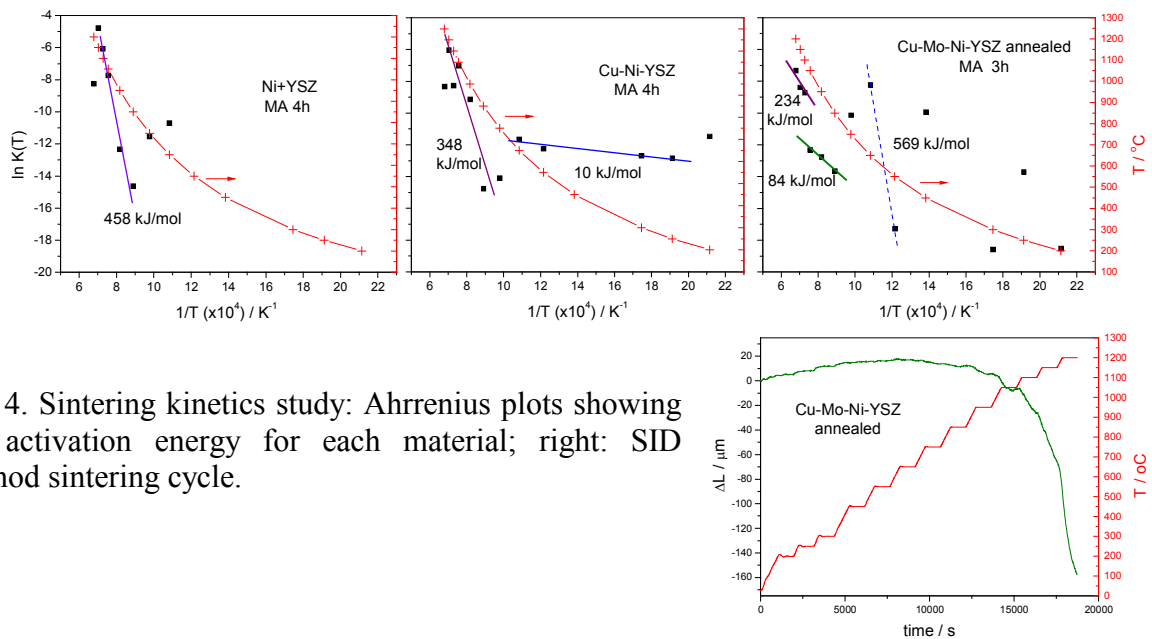


Fig. 4. Sintering kinetics study: Arrhenius plots showing the activation energy for each material; right: SID method sintering cycle.

The annealing treatment of the starting metallic powders clearly promotes the densification once it allows thin metallic coating over the ceramic particles approaching the pod-like powder morphology.

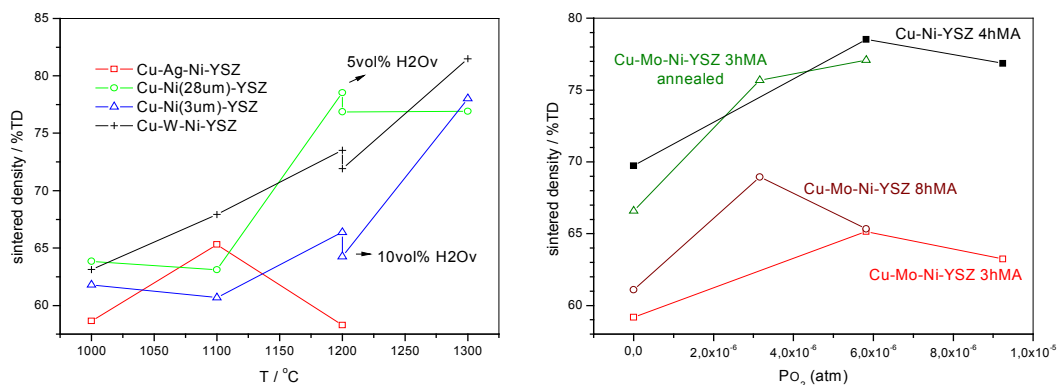


Fig. 5. SAS sintering process experiments at 1200°C/1h under controlled oxygen partial pressure moist atmosphere; samples processed by MA in different conditions.

The sintered microstructures observed by SEM (Fig. 6) reveal suitable features for applications as SOFC electrodes, say, refined microconstituents and porosity. The Mo bearing material shows a thin continuous metallic network while W is precipitated in some particle extremities (white field). The phase continuity is expected to assure good electrical and ionic percolation. Fig. 7 shows the electrical and thermal conductivity results measured for the main samples. The sample Cu-Ni-YSZ is slightly superior than the Mo bearing one, although they are roughly similar. There is an important gain regarding the conventional electrode material Ni-YSZ.

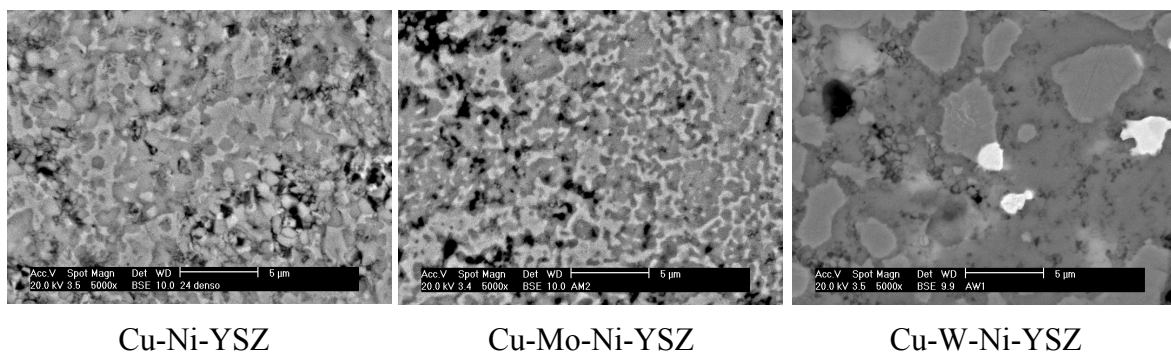


Fig. 6. Sintered microstructures.

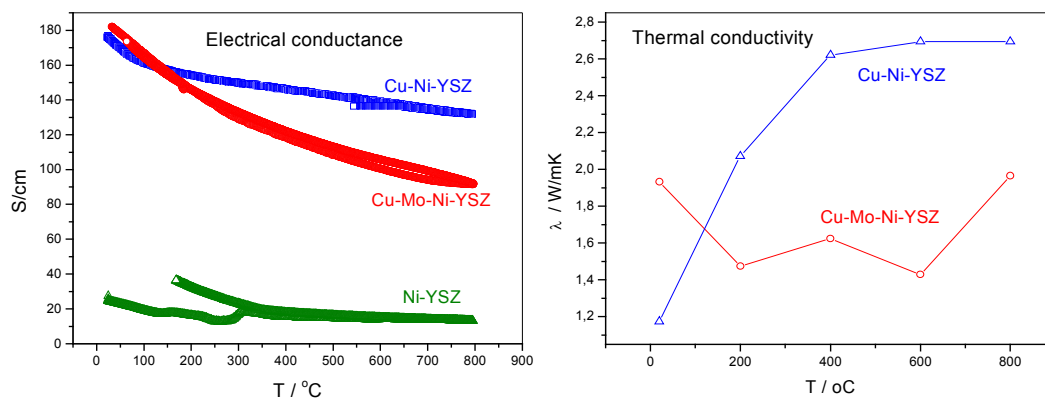


Fig. 7. Electrical and thermal conductivity.

Conclusions

Mechanical alloying has been validated as a new route for cermet preparation with good properties and suitable microstructure. The conceptual sintering by activated surface process is based on microplating metallic films to protect the ceramic surfaces, which are subsequently removed and exposes fresh ceramic and metallic surfaces of high activity. The SAS projected model has been proved through sintering experiments under controlled oxygen partial pressure as well as kinetic studies. A great sintering temperature reduction can be obtained exceeding 300°C.

The authors acknowledge the research councils FAPESP, CNPq, FINEP and CAPES for the financial support.

References

- [1] A. Atkinson, et al. *Nature Materials*, Vol 3, Issue 1, jan 2004, 17-27.
- [2] N.Q. Minh *J. Am. Ceram. Soc.* 76 [3], 563-88 (1993).
- [3] J.D. Holladay et al. *Catalysis Today* 139 (2009) 244–260.
- [4] R. Hino et al.. *Nuclear Engineering and Design* 233 (2004) 363–375
- [5] H. S. Hong, U. Chae, S. Choo. *Journal of Alloys and Compounds*, 449, 1-2, (2008), 331-334.
- [6] Kyoung-Hoon Kang, et al. *Journal of Alloys and Compounds* 448 (2008) 363–367.
- [7] H.S. Hong, et al. *Journal of Power Sources* 149 (2005), 84–89.
- [8] H.S. Hong et al. *Materials Science Forum* Vols. 486-487 (2005), 662-665.
- [9] S. Lee et al. *J. Alloys Compd.* (2007), doi:10.1016/j.jallcom.2007.08.022
- [10] R. Wilkenhoener. *Journal Of Materials Science* 34 (1999), 257– 265.
- [11] H. J. Cho, G. M. Choi, *Journal of Power Sources* 176 (2008), 96–101.
- [12] T.A.G. Restivo, S.R.H. Mello-Castanho. *Journal of Power Sources* 185 (2008), 1262–1266.
- [13] T.A.G. Restivo, S.R.H. Mello-Castanho. *Materials Science Forum* 591-593 (2008), 514-520.
- [14] M.D. Gross, J.M. Vohs, R.J. Gorte. *Electrochimica Acta*, 52 (5) (2007), 1951-57.
- [15] C. Sun, U.J. Stimming. *Power Sources* (2007), oi:10.1016/j.jpowsour.2007.06.086.
- [16] Y. Fukai. *The Metal-Hydrogen System*. Springer, 1993.
- [17] T.A.G. Restivo. Tese de Doutorado, Escola Politécnica USP, 106p. (2003).
- [18] T.A.G. Restivo. Capocchi, J.D.T., *J. Nuclear Materials* 334, 189-194 (2004).
- [19] O. T. Sorensen. *J. Thermal Analysis*, vol. 38, 213-228, 1992.
- [20] P. L. Husum, O. T. Sorensen. *Thermochimica Acta*, vol.114, 131-138, 1987.
- [21] C. C. Guedes e Silva, F.M.S. Carvalho, T.A.G. Restivo. *Estudo dos Mecanismos de Difusão em Cerâmicas a Base de Alumina*. In: 14^a CBECIMAT, São Pedro, SP, Brasil, (2000)
- [22] T.A.G. Restivo, L. Pagano Jr. *Sintering studies on the UO₂.Gd₂O₃ system using SID method*, In: *Conference on Characterization and Quality Control of Nuclear Fuels 2002*, Hyderabad, India, 2003.
- [23] T.A.G. Restivo, L. Pagano Jr. *Effect of Additives on The Sintering Kinetics of The UO₂. Gd₂O₃ System*, In: *TCM Brussels*, 2003.
- [24] M. El Sayed Ali, O.T. Sorensen. *Riso-R-518* (1985). 12p.
- [25] H. Wang, O.T. Sorensen et al. *J. Am. Ceram. Soc.* 81 [3] 781-84 (1998).
- [26] O. Bellon, *Dilatometric Sintering Studies of Zirconia Toughened Ceramics*. Ecole Nationale Supérieure de Ceramiques Industrielles. Risoe National Laboratory. 1991.
- [27] R. Yan et al. *Materials Letters* 60 (2006) 3605–360.
- [28] A. Degiovanni et al. *Thermal Quadrupoles. Solving the Heat Equation Through Integral Transforms*. John Wiley & Sons, Ltd, 2000, ISBN 0 471 98320 9.
- [29] T.A.G. Restivo. *Final Technical Report - code C6/BRA0030/P*. Vienna:IAEA, 2001.
- [30] O. Kubaschewski, C.B. Alcock, P.J. Spencer. *Materials Thermo-Chemistry*, 6th Ed., Pergamon, 1993.